

## DRIVING SOLAR SPICULES AND JETS WITH MAGNETOHYDRODYNAMIC TURBULENCE: TESTING A PERSISTENT IDEA

STEVEN R. CRANMER<sup>1</sup> AND LAUREN N. WOOLSEY<sup>2</sup>

Draft version October 24, 2018

### ABSTRACT

The solar chromosphere contains thin, highly dynamic strands of plasma known as spicules. Recently, it has been suggested that the smallest and fastest (Type II) spicules are identical to intermittent jets observed by the *Interface Region Imaging Spectrograph*. These jets appear to expand out along open magnetic field lines rooted in unipolar network regions of coronal holes. In this paper we revisit a thirty-year-old idea that spicules may be caused by upward forces associated with Alfvén waves. These forces involve the conversion of transverse Alfvén waves into compressive acoustic-like waves that steepen into shocks. The repeated buffeting due to upward shock propagation causes nonthermal expansion of the chromosphere and a transient levitation of the transition region. Some older models of wave-driven spicules assumed sinusoidal wave inputs, but the solar atmosphere is highly turbulent and stochastic. Thus, we model this process using the output of a time-dependent simulation of reduced magnetohydrodynamic turbulence. The resulting mode-converted compressive waves are strongly variable in time, with a higher transition region occurring when the amplitudes are large and a lower transition region when the amplitudes are small. In this picture, the transition region bobs up and down by several Mm on timescales less than a minute. These motions produce narrow, intermittent extensions of the chromosphere that have similar properties as the observed jets and Type II spicules.

*Keywords:* Sun: atmosphere – Sun: chromosphere – Sun: corona – turbulence – waves

### 1. INTRODUCTION

The Sun’s hot corona expands into interplanetary space as a supersonic plasma outflow known as the solar wind. However, we still do not yet know how the tenuous corona/wind system is formed from the much larger pool of mass and energy in the colder photosphere and chromosphere. High-resolution observations (e.g., Fletcher et al. 2015) show that coronal heating is highly dynamic and intermittent in space and time. Some have suggested that much of the corona’s mass and energy may be injected in the form of narrow features known variously as spicules, fibrils, and mottles (Beckers 1972; Sterling 2000; De Pontieu et al. 2007; Tsiropoula et al. 2012). Recently, the *Interface Region Imaging Spectrograph* (*IRIS*, De Pontieu et al. 2014a) found similar jet-like features emerging from largely unipolar network flux concentrations in coronal holes and quiet regions on the solar surface (Tian et al. 2014, 2015).

Coronal holes have long been known to play host to narrow, ray-like features known as polar plumes and polar jets (Newkirk & Harvey 1968; Ahmad & Withbroe 1977; Wang et al. 1998; Dobrzycka et al. 2002; Culhane et al. 2007; Raouafi et al. 2008; Young & Muglach 2014; Paraschiv et al. 2015). These bright strands typically extend up to heights of order 0.1–1  $R_{\odot}$ , whereas spicules and the *IRIS* network jets have length scales of only  $\sim 0.01 R_{\odot}$ . The largest plumes and jets are often associated with the emergence of small magnetic loops at their footpoints, and thus they are believed to be powered by magnetic reconnection (see, e.g., Wang & Sheeley 1995; Shibata et al. 2007; Pariat et al. 2009; Moore et al. 2010; Cheung et al. 2015). However, no clear evidence for reconnection in the smaller *IRIS* jets has been found so far.

In this paper we explore the idea that magnetohydrodynamic (MHD) waves are responsible for producing rapidly varying, field-aligned extensions of cool chromospheric gas along network flux tubes in coronal holes. These modeled features are found to have similar properties as the *IRIS* network jets, which Tian et al. (2014) proposed to be identical to the so-called Type II spicules observed above the limb. The idea that spicules could be driven by MHD waves has been discussed for several decades (Hollweg et al. 1982; Mariska & Hollweg 1985; Hollweg 1992; Kudoh & Shibata 1999; De Pontieu 1999; Velli & Liewer 1999; Matsumoto & Shibata 2010; Murawski et al. 2015), but it is still not known whether this is a dominant mechanism in the real solar atmosphere.

Many of the necessary ingredients of the wave-driven spicule model are supported by observations. The solar corona contains transverse, incompressible oscillations in the magnetic field and plasma velocity (Banerjee et al. 1998; Tomczyk et al. 2007; Jess et al. 2009; McIntosh 2012), but whether they should be called “Alfvén waves” is still a matter of debate (e.g., Mathioudakis et al. 2013). More specifically, spicules and jets themselves seem to contain torsional or kink motions that could have an Alfvénic character (Kukhianidze et al. 2006; De Pontieu et al. 2014b; Tavabi et al. 2015). There is also evidence for longitudinal compressive waves—i.e., fluctuations in density and the velocity component parallel to the wavenumber vector—that may or may not follow the ideal MHD magnetoacoustic dispersion relations (Ofman et al. 1999; Krishna Prasad et al. 2012; Threlfall et al. 2013; Miyamoto et al. 2014). In polar plumes, Liu et al. (2015) found high-frequency Alfvén-like waves and low-frequency compressive waves traveling along the same field lines, which points to the possibility of mode coupling. Also, Pant et al. (2015) found what appear to be slow-mode magnetosonic waves within the *IRIS* network jets.

The models developed in this paper rely on MHD waves behaving in an intermittent and stochastic manner. Several ear-

<sup>1</sup> Department of Astrophysical and Planetary Sciences, Laboratory for Atmospheric and Space Physics, University of Colorado, Boulder, CO 80309, USA

<sup>2</sup> Harvard-Smithsonian Center for Astrophysics, 60 Garden Street, Cambridge, MA 02138, USA

lier attempts to understand spicules as a by-product of waves assumed a periodic, sinusoidal driver at the lower boundary of the modeled system. However, both observations (Tomczyk & McIntosh 2009; Liu et al. 2014) and simulations (e.g., van Ballegoijen et al. 2011; Perez & Chandran 2013; Zhdankin et al. 2015) show that MHD fluctuations in the chromosphere and corona exhibit continuous power-law spectra and irregular bursts of activity and dissipation. This variability may also be related to the fact that the Sun’s transition region (TR) has a complex “corrugated” shape (Feldman et al. 1979; Zhang et al. 1998; Peter 2013). We propose that jets and Type II spicules are short-lived extensions of the corrugated TR that are driven by similarly infrequent outliers in the underlying population of waves and turbulent eddies.

The remainder of this paper is organized as follows. Section 2 discusses how chromospheric Alfvén waves may evolve nonlinearly into a collection of compressible fluctuations. In Section 3 we estimate the degree of nonthermal expansion experienced by the upper chromosphere and TR as a result of shocks that develop from a compressive wave train. Section 4 takes the output from a reduced MHD simulation of Alfvénic turbulence in a coronal hole and computes the time-dependent generation of compressive waves and intermittent levitation of the TR. In Section 5 we compare the modeled up-and-down motions of the TR with the observed properties of Type II spicules and *IRIS* network jets. Lastly, in Section 6 we summarize our results, discuss some broader implications, and describe future improvements to the models.

## 2. NONLINEAR PRODUCTION OF PARALLEL VELOCITY FLUCTUATIONS

When incompressible Alfvénic fluctuations grow to a sufficiently large amplitude (i.e., when the oscillating transverse magnetic field  $\delta B_{\perp}$  becomes of the same order of magnitude as the background field strength  $B_0$ ), they become susceptible to a range of nonlinear interactions that can spawn other types of waves. For example,

1. It has been known for several decades that linearly polarized Alfvén waves can excite second-order *ponderomotive oscillations* in density, gas pressure, and magnetic pressure (Hollweg 1971; Spangler 1989; Vasquez & Hollweg 1996). Because these oscillations are tied to the extrema of transverse arcs traced by the magnetic field vector, their frequencies tend to be twice those of the original Alfvén wave. Corresponding wave periods, for Alfvén waves oscillating with  $\mathcal{P}_A \approx 3\text{--}5$  minutes, are of order 1–2 minutes. These are reminiscent of the durations and recurrence timescales of Type II spicules.
2. There has also been substantial work done to study the nonlinear development of *parametric instabilities* for circularly polarized Alfvén waves (Goldstein 1978; Jayanti & Hollweg 1993; Turkmani & Torkelsson 2003; Del Zanna et al. 2015). For conditions appropriate to the corona, this instability usually involves an upward propagating Alfvén wave decaying into a downward propagating Alfvén wave and an upward propagating magnetosonic-like wave. The latter tends to have a lower frequency  $\omega_S$  than that of the original Alfvén wave  $\omega_A$ . Typical periods ( $\mathcal{P} = 2\pi/\omega$ ) in the open-field corona are

$$\mathcal{P}_S \approx \left( \frac{V_A}{2c_s} \right) \mathcal{P}_A \quad (1)$$

which for  $\mathcal{P}_A \approx 3$  minutes, typical coronal Alfvén speeds  $V_A \approx 2000 \text{ km s}^{-1}$ , and sound speeds  $c_s \approx 150 \text{ km s}^{-1}$ , gives a period of order 20 minutes, similar to what is observed for density fluctuations above the limb (e.g., Ofman et al. 1999; Threlfall et al. 2013).

The number of possible mode-coupling interactions grows even bigger when the MHD waves pass through a strongly inhomogeneous background medium (e.g., Heyvaerts & Priest 1983; Lee & Roberts 1986; Nakariakov et al. 1998; Hollweg & Kaghshvili 2012; Thurgood & McLaughlin 2013).

Because we are concerned with the development of short-lived spicules and jets along unipolar field lines, we focus on the most rapid kind of nonlinear mode coupling that occurs in homogeneous plasmas: the second-order ponderomotive effect. Hollweg (1971) showed that large-amplitude linearly polarized Alfvén waves produce an oscillation  $\delta v_{\parallel}$  in the parallel velocity with an amplitude that scales as

$$\frac{\delta v_{\parallel}}{V_A} = N_{\beta} \left( \frac{\delta B_{\perp}}{B_0} \right)^2, \quad (2)$$

where  $N_{\beta}$  describes the dependence on the plasma  $\beta$  parameter. We use a simplified kinetic definition of  $\beta = (c_s/V_A)^2$  which is different by a factor of  $2/\gamma \approx 1.2$  from the standard MHD definition of the ratio of pressures. Hollweg (1971) used the ideal MHD conservation equations to derive

$$N_{\beta} = \frac{0.25}{|1-\beta|}, \quad (3)$$

which diverges unrealistically at the asymptotic value of  $\beta = 1$ . Vasquez & Hollweg (1996) extended the second order MHD theory and found, for some cases,  $N_{\beta} = 0.25/(1+\beta)$ . Several other properties of this solution were consistent with a magnetosonic-like wave mode.

A substantial amount of other theoretical work has been done to simulate the nonlinear evolution of Alfvén waves, much of which involves solving the Derivative Nonlinear Schrödinger (DNLS) equation (e.g., Mjølhus & Wyller 1986; Medvedev & Diamond 1996). In this paper, we make use of the kinetic results of Spangler (1989), who solved a perturbed Vlasov equation for the ponderomotive density fluctuations associated with a soliton-like Alfvén pulse. We solved the Spangler (1989) equations for a range of plasma  $\beta$  values and for the simple one-temperature case of  $T_e = T_p$ . Effective compressional amplitudes were extracted from the simulated density fluctuation profiles, which did not maintain the same Lorentzian shape of the input Alfvénic pulse. We maintained continuity with earlier studies of sinusoidal waves by computing the relative fluctuation ratio  $\delta\rho/\rho_0$  as half the peak-to-peak pulse variation in density. Also, we assumed the acoustic-like energy equipartition found by Hollweg (1971),

$$\frac{\delta v_{\parallel}}{V_A} = \frac{\delta\rho}{\rho_0} \quad (4)$$

and used it to compute  $\delta v_{\parallel}$  as in Equation (2). The numerical results were used to construct the efficiency factor  $N_{\beta}$ , and Figure 1 shows its dependence on  $\beta$ . This function agrees with the above analytic results in the limits of  $\beta \ll 1$  and  $\beta \gg 1$ , and it falls in between them for  $\beta \approx 1$ . We fit the  $\beta$  dependence of this factor by an approximate function,

$$N_{\beta} \approx \frac{0.25}{\sqrt{1+\beta^2}} + \frac{0.135\beta^{2.4}}{0.305+\beta^{4.6}} \quad (5)$$

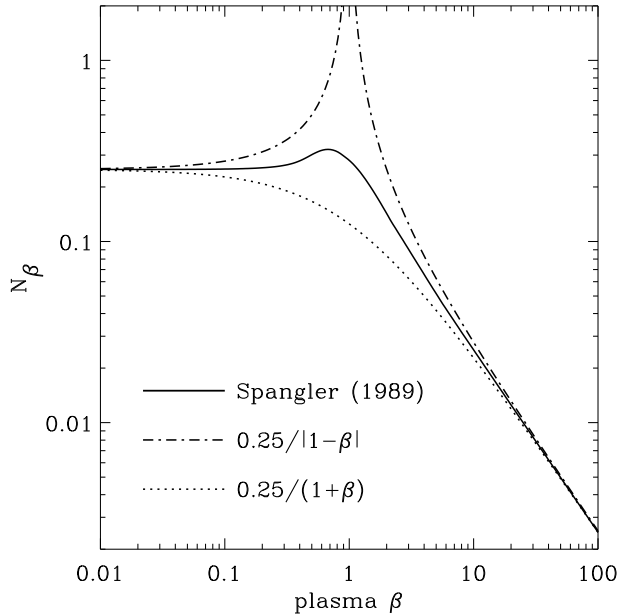


**Figure 1.** Dependence of the dimensionless mode-conversion efficiency  $N_\beta$  on the kinetic plasma  $\beta$ , including results from [Hollweg \(1971\)](#) (dot-dashed curve), [Vasquez & Hollweg \(1996\)](#) (dotted curve), and present work based on [Spangler \(1989\)](#) (solid curve).

and this is accurate to within about 3% over the range of  $\beta$  values shown in Figure 1. A plot of this function would be nearly indistinguishable from the solid curve that shows the numerical results of the [Spangler \(1989\)](#) model.

Later in this paper, Equations (2), (4), and (5) are used to compute the properties of acoustic-like waves that are generated from a time-dependent simulation of Alfvénic turbulence in the chromosphere and low corona. We find that there is a distinct local maximum in  $\delta v_{\parallel}$  at a height  $z_b = 876$  km in the low chromosphere. That location will be taken as a conceptual “base height” and used to compare against other models of acoustic wave evolution.

### 3. SHOCK STEEPENING AND CHROMOSPHERIC LEVITATION

In the solar chromosphere, upwardly propagating acoustic waves undergo rapid growth in amplitude, with  $\delta v_{\parallel} \propto \rho_0^{-1/2}$  in the limit of an isothermal atmosphere and no dissipation ([Lamb 1908, 1932](#)). At some point, however, the amplitudes become large enough for the waves to steepen into shocks (e.g., [Stein & Schwartz 1972](#)) and thereby dissipate their energy into the surrounding atmosphere. In the process of damping, the fluctuations are also able to exert a mean upward *wave pressure gradient* force on the atmosphere ([Dewar 1970; Jacques 1977](#)). This force is essentially a net transfer of momentum from the oscillations to the background gas. In a hydrostatic atmosphere (or in the subsonic parts of the solar wind), an increase in the total effective pressure increases the gravitational scale height, and this in turn “puffs up” the cool chromosphere. This effect has also been explored in the context of atmospheres of cool, evolved giant stars (see, e.g., [Bertschinger & Chevalier 1985; Ludwig & Kučinskás 2012](#)).

We simulated the above chain of events using a series of one-dimensional time-steady solutions of the ZEPHYR code ([Cranmer et al. 2007](#)). This code produces a realistic description of the photosphere, chromosphere, corona, and solar wind in open-field regions of the solar atmosphere. ZEPHYR solves equations of wave action conservation for both acous-

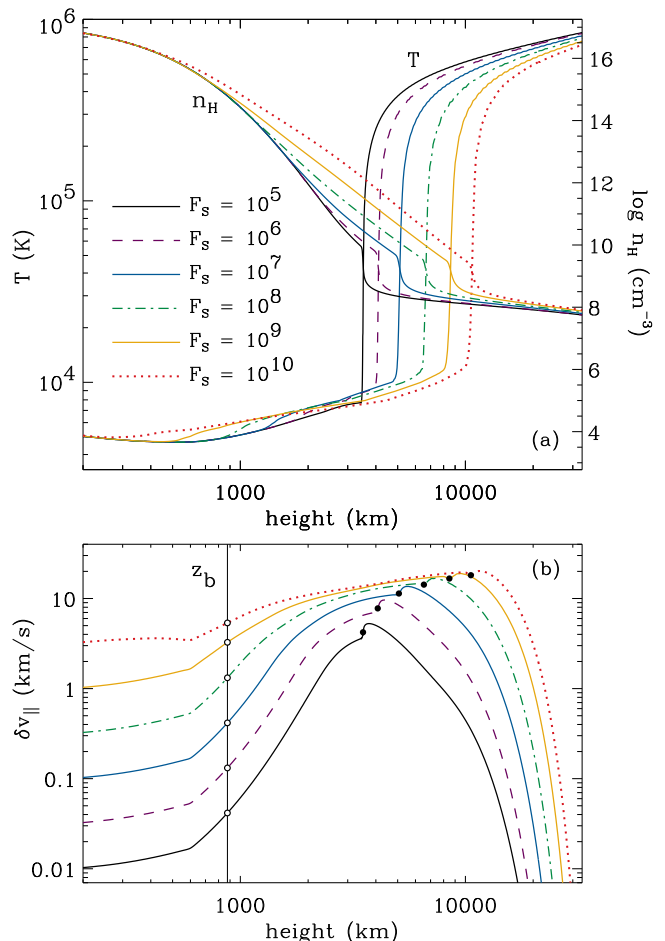


**Figure 2.** Height dependence of (a) time-steady temperatures  $T$  and hydrogen number densities  $n_H$ , and (b) acoustic wave velocity amplitudes  $\delta v_{\parallel}$ , corresponding to a set of ZEPHYR models with a range of acoustic wave fluxes  $F_S$ . Line colors/styles denote  $F_S$  (see caption) and are consistent in both panels. Also shown are the chromospheric base height  $z_b$  (white circles) and transition region height  $z_{TR}$  (black circles).

tic and Alfvén waves in the presence of several kinds of dissipation and shock steepening, and it includes wave pressure terms that couple the fluctuations to the background plasma. In these models there is no coupling between the acoustic and Alfvén wave modes; they each evolve independently of one another. Specifically, we made use of the grid of models from Section 8.2 of [Cranmer et al. \(2007\)](#), in which the Alfvén wave properties were held fixed and the acoustic wave flux at the photospheric boundary was varied over several orders of magnitude.

Figure 2 summarizes the results from the ZEPHYR models with a range of acoustic wave power inputs. Figure 2(a) shows the time-steady variation of density and temperature with height, and Figure 2(b) shows how the root-mean-squared (rms) parallel velocity amplitude  $\delta v_{\parallel}$  varies with height for these models. As the acoustic waves become stronger, the chromospheric scale height receives an increasingly large augmentation from wave pressure. In the models of [Cranmer et al. \(2007\)](#), the sharp TR between chromospheric and coronal temperatures occurs when the density dips below a critical value determined by the peak of the optically thin radiative loss function (see also [Owocki 2004](#)). The models with stronger acoustic waves have flatter density gradients, so the critical density is reached at larger heights.

**Table 1**  
Chromospheric Properties of ZEPHYR Models

$F_S$ (erg s <sup>-1</sup> cm <sup>-2</sup> )	$\delta v_{\parallel}(z_b)$ (km s <sup>-1</sup> )	$\delta v_{\parallel}(z_{\text{TR}})$ (km s <sup>-1</sup> )	$z_{\text{TR}}$ (km)	$u_{1\text{AU}}$ (km s <sup>-1</sup> )	$\dot{M}$ ( $M_{\odot}/\text{yr}$ )
0	0	0	3364	723	$1.91 \times 10^{-14}$
$10^5$	0.0416	4.22	3508	722	$1.91 \times 10^{-14}$
$10^6$	0.132	7.77	4078	724	$1.88 \times 10^{-14}$
$10^7$	0.416	11.4	5062	720	$1.90 \times 10^{-14}$
$10^8$	1.32	14.3	6540	720	$1.88 \times 10^{-14}$
$10^9$	3.26	16.7	8484	721	$1.86 \times 10^{-14}$
$10^{10}$	5.36	18.1	10576	728	$1.76 \times 10^{-14}$

Table 1 lists some key properties of each ZEPHYR model. The acoustic wave energy flux  $F_S$  is injected at the photospheric lower boundary, and the velocity amplitudes  $\delta v_{\parallel}$  increase monotonically with increasing height from the photosphere to the TR. Between the photosphere ( $z = 0$ ) and the TR height ( $z_{\text{TR}}$ ) we focus on the lower chromospheric base height  $z_b = 876$  km and highlight it with a vertical line in Figure 2(b). The TR is defined as the height at which the modeled temperature  $T$  first rises to 20,000 K. This is lower than the temperatures at which most TR emission lines are formed, but we are using  $z_{\text{TR}}$  as an effective height for the tips of spicules and jets; i.e., where chromospheric emission ends.

The time-averaged shock-driven levitation of the TR is a key result of the models shown in Figure 2. Without any compressive waves, the Sun’s TR occurs in the models at a height of  $\sim 3300$  km above the photosphere. This is slightly higher than the canonical range of 2000–2500 km that is seen in one-dimensional empirical models (e.g., Vernazza et al. 1981; Avrett & Loeser 2008). With increasing “turbulent pressure,” the modeled  $z_{\text{TR}}$  can increase to values greater than 10,000 km. Table 1 gives a span of heights between these extremes, and these are roughly consistent with the values sometimes reported from off-limb chromospheric measurements (Zhang et al. 1998; Filippov & Koutchmy 2000). In any case, we use the results given in Table 1 as an interpolation lookup table that provides an instantaneous estimate of  $z_{\text{TR}}$  for any given value of  $\delta v_{\parallel}(z_b)$ .

In the upper chromosphere, the acoustic waves begin to dissipate because they steepen into shocks. The time-averaged damping rate is dominated by the entropy change  $T\Delta S$  at each shock, spread out over the time between successive shock passages. The models with larger values of  $F_S$  undergo steepening at lower heights, so their chromospheric profiles of  $\delta v_{\parallel}(z)$  become flatter and more saturated. Above the TR, the acoustic waves damp rapidly due to the greatly amplified rate of heat conduction in the corona (see, e.g., Equation (26) of Cranmer et al. 2007). Because of this rapid damping, the acoustic waves have a negligible effect on the eventual acceleration of the fast solar wind.<sup>3</sup> Note from Table 1 that the wind speed at 1 AU and the sphere-averaged mass loss rate  $\dot{M}$  are barely affected by changing  $F_S$ .

Below, we make use of the correlation seen in Table 1 between  $\delta v_{\parallel}(z_b)$  and  $z_{\text{TR}}$ . This is applied to a time-dependent simulation of incompressible turbulence that does *not* contain acoustic waves driven at the photosphere. Instead, we

<sup>3</sup> However, Nuevo et al. (2013) suggested that the rapid damping of compressive waves may have a strong impact on the coronal heating in large hydrostatic loops. With enough energy dissipated at low heights, the maximum temperature may occur below the loop apex, thus giving rise to loops with decreasing  $T(z)$  in the corona.

assume that compressive waves are generated throughout the chromosphere by the nonlinear mode conversion mechanism discussed in Section 2. We assume that the upward evolution of those compressive waves produces a shock-driven levitation similar to that seen in the ZEPHYR models. Of course, it should be made clear that the second-order variations in  $\delta v_{\parallel}$  described by Equation (2) are not identical to classical sound waves; e.g., they propagate at a phase speed of  $V_A$  instead of  $c_s$ . However, once these waves steepen into shocks, the time-averaged loss of momentum and energy is expected to be similar to the acoustic-wave case.

#### 4. RESULTS FROM TIME-DEPENDENT MHD TURBULENCE

Although the ZEPHYR code simulates the transport, cascade, and dissipation of Alfvénic turbulence, it does so using time-averaged phenomenological equations. These equations do not self-consistently simulate the actual process of an MHD cascade, which is believed to be a consequence of partial wave reflections and nonlinear interactions between Alfvén wave packets. In order to more accurately model these processes, a time-dependent and three-dimensional approach is needed. We used a reduced MHD (RMHD) code called BRAID (van Ballegooijen et al. 2011; Asgari-Targhi & van Ballegooijen 2012; Asgari-Targhi et al. 2013; van Ballegooijen et al. 2014) that simulates the generation and evolution of incompressible turbulence along an expanding flux tube with a circular cross section. This code has successfully simulated the intermittent and dynamic heating seen in the chromospheric and coronal regions of closed loops. Also, Skogsrud et al. (2014) proposed that this type of turbulence model may explain the complex multi-threaded dynamics seen within Type II spicules.

We used the simulation of an open coronal-hole flux tube developed by Woolsey & Cranmer (2015). The BRAID coronal hole model extends from the solar photosphere ( $z = 0$ ) to a maximum height of  $z = 2R_{\odot}$ . The choice of the latter value was a compromise between wanting to model as much of the solar wind’s acceleration region as possible and the fact that the RMHD equations in BRAID do not yet include the background outflow speed (i.e., they assume the wind speed  $u \ll V_A$ , which breaks down above a few solar radii). The model was run for 2300 s of simulation time, which corresponds to about three times the Alfvén wave travel time through the radial grid.

The background properties of the BRAID model (e.g.,  $B_0$ ,  $V_A$ ,  $c_s$ ) are the same as in the time-steady polar coronal hole model of Cranmer et al. (2007). Figure 3 shows a selection of these quantities from the upper photosphere ( $z = 100$  km) to the low corona. Note that this is specifically a model of a vertical flux tube rooted in the bright supergranular network; the field strength  $B_0$  remains greater than 100 G until one reaches a height of about 1100 km. The magnetized network chromosphere (above the so-called “merging height” where individual intergranular flux tubes join together) can be seen in Figure 3 as a region of rapidly decreasing  $\beta$  with increasing height.

Figures 3(a) and 3(b) show the time-averaged amplitudes of transverse fluctuations in velocity and magnetic field, respectively. As described further by Woolsey & Cranmer (2015), the rms averaging in these cases was performed in two steps: (1) the variance was taken over all 92 discrete RMHD spectral wave modes at each height and time step, then (2) the variance over simulation time was computed at each height, excluding the earliest time steps during which the base-driven waves had

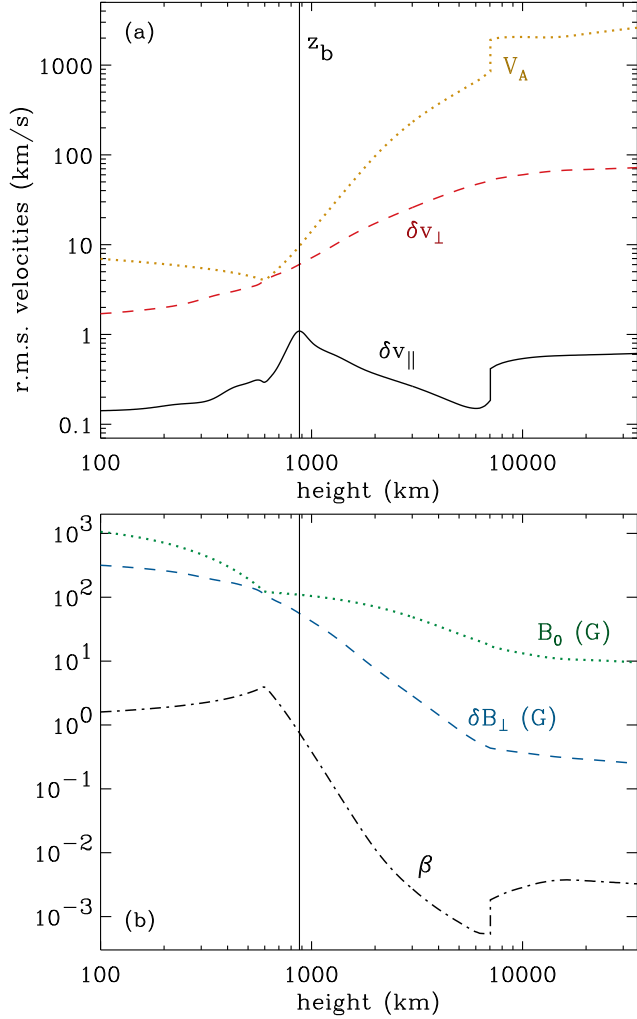


**Figure 3.** Time-averaged plasma properties in the BRAID model of coronal hole network: (a) Alfvén speed  $V_A$  (gold dotted curve), rms transverse velocity amplitude  $\delta v_{\perp}$  (red dashed curve), rms longitudinal compressive wave amplitude  $\delta v_{\parallel}$  (solid black curve). (b) background magnetic field strength  $B_0$  (green dotted curve), rms transverse magnetic field amplitude  $\delta B_{\perp}$  (blue dashed curve), plasma  $\beta$  ratio (black dot-dashed curve). As in Figure 2(b), the base height  $z_b$  is highlighted by a vertical line.

not yet traversed the grid. Note that the BRAID fluctuations do not obey ideal MHD energy equipartition; it is possible for the energy densities in the kinetic and magnetic fluctuations to be unequal to one another. It is clear that the conditions in the upper chromosphere (around  $z_b$ ) appear to be optimal for strong nonlinear mode conversion; not only is  $\beta \approx 1$ , but also  $\delta B_{\perp} \approx B_0$ .

To focus on the region(s) of the chromosphere and corona in which the mode conversion is strongest, we applied Equation (2) to the time-averaged rms properties shown in Figure 3. The resulting height dependence of the rms  $\delta v_{\parallel}$  amplitude is also plotted in Figure 3(a). There is a clear peak in the low chromosphere at a height of 876 km, with a maximum amplitude of  $\sim 1$  km s $^{-1}$ . This location is defined as the base height  $z_b$ , and we consider it as an effectively localized chromospheric “source” of compressive waves.

Next we examine the highly variable and intermittent nature of the BRAID turbulence at a fixed height. Specifically, at the base height  $z_b$ , the fluctuations were averaged over all 92 spectral wave modes (i.e., integrated over the  $k_{\perp}$  power spec-

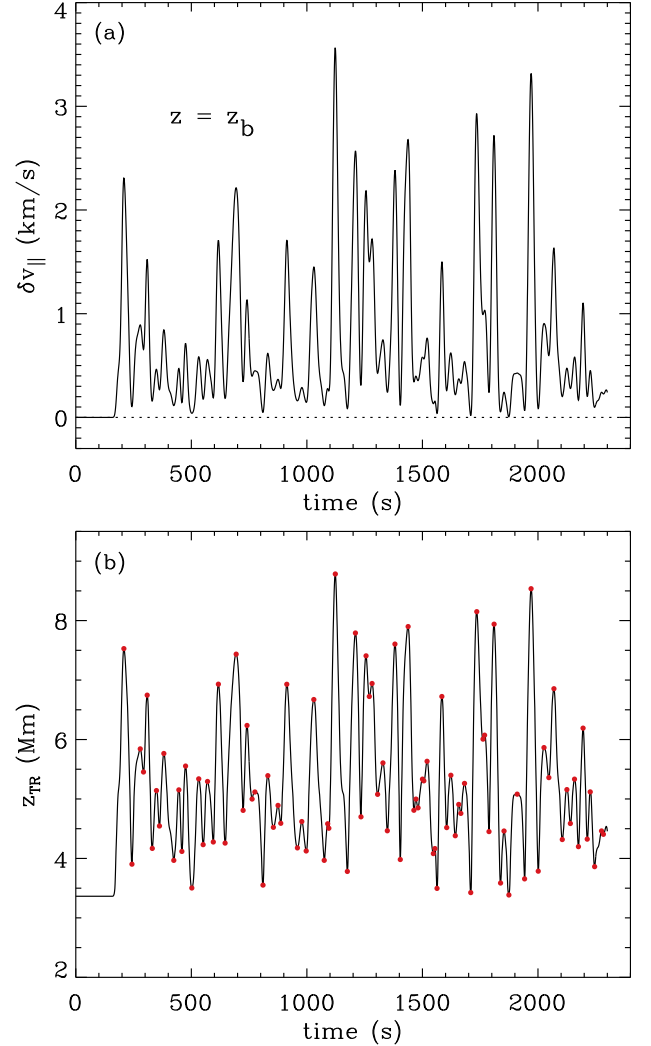


**Figure 4.** BRAID-model time dependence of: (a) the simulated compressive wave amplitude  $\delta v_{\parallel}$  at the base height  $z_b$ , and (b) the instantaneous TR height  $z_{\text{TR}}$  corresponding to the variable  $\delta v_{\parallel}$ . Individual maxima and minima in  $z_{\text{TR}}$  are highlighted with red circles.

trum), but not over time. At this height, the mean value of the RMHD Alfvén velocity amplitude is  $\delta v_{\perp} = 5.03$  km s $^{-1}$ , with a standard deviation of 2.92 km s $^{-1}$  and a long tail in the distribution that extends up to a maximum value of 13.9 km s $^{-1}$ . For comparison, the Alfvén speed  $V_A$  and sound speed  $c_s$  at this height are 9.64 km s $^{-1}$  and 8.35 km s $^{-1}$ , respectively. A similarly processed time series of the ratio  $\delta B_{\perp}/B_0$  has a mean of 0.45 at this height, a standard deviation of 0.21, and a maximum value of 1.08.

Figure 4(a) shows the result of applying Equation (2) to estimate the time dependence of  $\delta v_{\parallel}$  at  $z_b$ . Note that this wildly fluctuating quantity is an actual *amplitude* and not the full time-dependence of the parallel velocity. If the input Alfvén wave had been a monochromatic sinusoidal oscillation, the estimated  $\delta v_{\parallel}$  amplitude would have been an unchanging constant. Also, because of the nonlinear nature of the mode conversion,  $\delta v_{\parallel}(t)$  ends up having a greater relative variability than either  $\delta v_{\perp}(t)$  or  $\delta B_{\perp}(t)$ . For these incompressible transverse amplitudes, the ratios of their standard deviations to their mean values are about 0.5–0.6. For the computed time series of  $\delta v_{\parallel}$ , this ratio is about 1.0.

Figure 4(b) shows the time dependence of  $z_{\text{TR}}$ , which we computed via straightforward interpolation from the ZEPHYR model properties given in Table 1. The TR height varies up and down with swings of order 2 to 5 Mm, which overlaps with the observed range of *IRIS* network jet lengths (Tian et al. 2014). Implicit in Figure 4(b) is the assumption that the upper chromosphere’s response to variability in  $\delta v_{\parallel}$  is more or less instantaneous. A more accurate model would have to include a finite relaxation time for the wave-pressure levitation to take effect. Because the compressive waves travel at a phase speed  $V_A$ , we anticipate that this relaxation time should be given roughly by the Alfvén-wave travel time from  $z_b$  to  $z_{\text{TR}}$ . This travel time is about 50 s, which is similar in magnitude to the recurrence time between the modeled oscillations in  $z_{\text{TR}}$ . Thus, even though future simulations are needed to verify these effects (see Section 6), we do not believe they will differ greatly from the simpler estimates made here.

### 5. INTERPRETATION: SPICULES AND JETS?

In the ZEPHYR models discussed in Section 3, the “steepened” acoustic wave amplitudes  $\delta v_{\parallel}$  at the TR were of order 5 to 20 km s<sup>-1</sup>. These velocities are small when compared to the observed velocities of Type II spicules and *IRIS* network jets. However, we see much larger *apparent* velocities when examining the upward and downward variations of  $z_{\text{TR}}$  in Figure 4(b). We compute these velocities by recording the minima and maxima in  $z_{\text{TR}}(t)$  and taking sequential finite differences between them in height ( $\Delta z$ ) and in time ( $\Delta t$ ). These minima and maxima are shown as red symbols in Figure 4(b). The apparent velocity for each jet-like event is then computed as  $V_{\text{jet}} = \Delta z / \Delta t$ . From the oscillatory nature of  $z_{\text{TR}}(t)$ , it is apparent that there will be roughly equal numbers of positive (low to high) and negative (high to low) values of  $V_{\text{jet}}$ . We eventually plan to simulate *IRIS*-like emission-line images of these evolving features, but doing so is beyond the scope of this paper. For now, we focus on the upward motions in  $z_{\text{TR}}$  (e.g., the 46 out of 93 cataloged events for which  $V_{\text{jet}} > 0$ ) and compare them to observed upward motions in Type II spicules and network jets.

Figure 5 shows how the modeled collection of positive  $V_{\text{jet}}$  values is correlated with their “lifetimes”  $\Delta t$ . We found in the list of 46 events that  $\Delta z$  is roughly proportional to  $\Delta t^2$ , so there is a roughly linear relationship between  $V_{\text{jet}}$  and  $\Delta t$ . In Figure 5 we also show reported ranges for the speeds and lifetimes of Type I and II spicules (Pereira et al. 2012) and *IRIS* network jets (Tian et al. 2014, 2015). The overlap between the properties of Type II spicules and network jets has led to a growing conjecture that these represent identical magnetic features that have been observed in different ways. It is clear that our modeled events with the highest speeds (corresponding also to the largest values of  $\Delta z$ ) have very similar properties as the observed features.

Figure 5 highlights modeled events with  $\Delta z \geq 2''$  (i.e.,  $\Delta z \geq 1.45$  Mm) with larger and darker symbols. This dividing line is close to the mean value of our distribution of simulated jet lengths, which exhibited a range between  $0.1''$  and  $7''$ . The open BRAID flux tube has a diameter that expands with increasing height, from about  $1''$  in the low chromosphere ( $z_b$ ) to  $3''$  at the largest heights shown in Figure 3. For comparison, the observed *IRIS* network jets have lengths between about  $3''$  and  $12''$ , and roughly constant widths of order  $0.5''$  (Tian et al. 2014, 2015). We believe that only events with  $\Delta z$  greater than their cross-sectional diameter would ac-

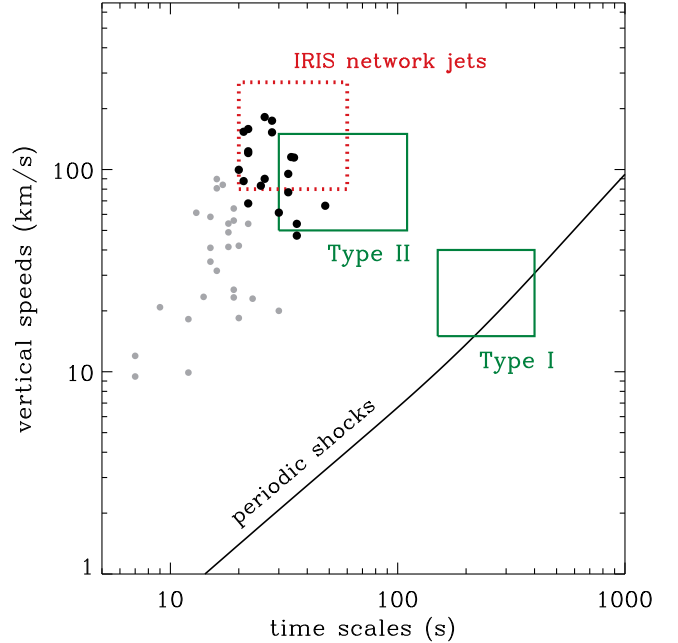


**Figure 5.** Two-dimensional diagram of representative time scales plotted versus vertical speeds. Observed ranges of parameters for Type I and II spicules (green solid-curve boxes) and *IRIS* network jets (red dotted-curve box) are compared with BRAID-model simulations of  $\Delta t$  and  $V_{\text{jet}}$ . Large black symbols show modeled events with lengths greater than  $2''$ , and small gray symbols show modeled events with lengths less than  $2''$ . The Bertschinger & Chevalier (1985) relationship for periodic shocks is shown with a solid black curve.

tually be observable as narrow jet-like enhancements in intensity. Thus, the darker symbols with  $\Delta z \geq 2''$  are meant to show only the events that would be distinctly noticeable as jets in, e.g., *IRIS* image sequences. Shorter jets (like the modeled events shown in light gray) may exist on the Sun, but they would likely be buried in the rapidly fluctuating background of the underlying chromospheric network.

The solid curve in Figure 5 shows the relationship between the initial upward velocities of shocks in a hydrostatic atmosphere and the recurrence timescale between successive shocks in a periodic train. We solved the semi-analytic equations given in Section II of Bertschinger & Chevalier (1985) for a range of Mach numbers between 1.1 and 30. In this model, gas is accelerated upward by each shock, then it tends to fall back down after the shock passes by. For periodic shock trains that obey the speed–timescale relation shown by the curve, each parcel of gas ends up at the same height one period later and executes cyclic motion. It is interesting that the properties of Type I spicules overlap with this critical curve, since they often appear to show parabolic trajectories in which parcels return to their original heights.

Regions to the left of the critical curve in Figure 5 correspond to shorter timescales than are required for cyclic motion. Thus, a given fluid parcel would encounter the “next” shock before it has fallen back to its original height. If the shock trains completely cover the stellar surface, such rapid recurrence would be associated with net mass loss (Willson & Hill 1979; Bertschinger & Chevalier 1985). Both Type II spicules and *IRIS* network jets occur in this region of parameter space, and it has been suggested that these features feed plasma into the corona and solar wind (e.g., De Pontieu et al. 2009; Tian et al. 2014). Chromospheric diagnostics of Type II spicules often show bright features moving up and not com-

ing back down (Pereira et al. 2012), but more recent coordinated observations with *IRIS* have shown some parabolic-like downflows (Skogsrud et al. 2015). Connections between observed features and the idealized periodic shock model of Bertschinger & Chevalier (1985) are instructive and suggestive, but they certainly do not tell the whole story.

## 6. DISCUSSION AND CONCLUSIONS

The goal of this paper was to explore one promising way that strong turbulence may produce dense, short-lived, and field-aligned extensions of chromospheric and TR plasma. We made use of a time-dependent RMHD model of Alfvénic turbulence in the coronal-hole network, and we took particular notice of the intermittent amplitude variability in the mid-chromosphere. At a height of about 900 km above the photosphere, the wave properties appear to be optimal to produce a spike of nonlinear mode conversion into longitudinal, compressive fluctuations. These waves have been shown to be able to “puff up” the effective density scale height of the chromosphere and thus temporarily increase the height of the TR. Using an existing grid of models, we computed the time-dependent TR height as an instantaneous response to the varying wave amplitudes and scale heights. Apparent upward velocities and recurrence timescales measured from the model time series agree quite well with the observed properties of *IRIS* network jets and Type II spicules.

There are other observable characteristics of jets and spicules that can, in principle, be compared with our models. Do the *IRIS* jets appear only for specific ranges of plasma properties in the upper chromosphere (i.e., those that maximize the mode conversion “spike” at  $z_b$ )? Is the observed filling factor of the jets (both in space and time) in agreement with the intermittency seen between the largest-amplitude pulses of  $\delta v_{\parallel}$  in Figure 4? These comparisons require robust statistics from the measurement of hundreds of individual jets and spicules. Collecting data with sufficient accuracy may require the use of automated feature-detection algorithms (e.g., Aschwanden et al. 2013).

We note that the models presented in this paper do not represent a completely self-consistent simulation of the proposed jet/spicule formation mechanism. Instead, we attempted to show—via a sequence of separate, simple, and well-understood models—that the various ingredients are present at the right order of magnitude to produce the proposed effects. We pay for this conceptual simplicity with the fact that the results (e.g., the up/down dynamics of the TR interface) are not likely to be quantitatively accurate. Full three-dimensional MHD simulations are required to test these ideas. Compressive simulations performed with fewer than three dimensions (e.g., Matsumoto & Suzuki 2014; Kono et al. 2015) already show suggestive hints of the relevant mode conversion from Alfvén waves to compressive/spicule-like pulses.

A comprehensive explanation for the *IRIS* jets and Type II spicules will also require taking into account some additional processes and complexities that we did not include. For example:

1. As described in Section 1, the larger polar plumes and jets are probably driven by magnetic reconnection at their footpoints. There may be an overlap between the smallest of these jets and the ones observed by *IRIS* in the (mostly) unipolar network (see also Moore et al. 2011). Coronal reconnection can also generate Alfvén waves (Hollweg 2006; Lynch et al. 2014),

and turbulence can also lead to the formation of small scale reconnecting current sheets (e.g., Matthaeus et al. 2015). The traditional dichotomy between wave-driven and reconnection-driven coronal heating theories is no longer so sharp, and it is useful to keep both kinds of processes in mind.

2. Our models assumed that open magnetic flux tubes in the coronal-hole network are essentially isolated from one another. However, there has been a great deal of work to study how wave-like fluctuations can enable the sharing of energy between neighboring flux tubes and their weak-field surroundings (e.g., Uchida & Kaburaki 1974; Roberts 2000; Bogdan et al. 2002; Hasan & van Ballegooijen 2008; Ofman 2009; Mumford et al. 2015). This is another type of “mode coupling” that needs to be taken into account.
3. We ignored parametric instabilities and nonlinear mode coupling that is enhanced by inhomogeneous background properties (see Section 2). The fact that we obtained the correct order-of-magnitude effect for the jet and Type II spicule properties may suggest that the adopted second-order ponderomotive coupling mechanism is dominant. However, the other proposed effects are likely to produce lower-frequency compressive waves that are the ones observed to survive to larger heights (see, e.g., Liu et al. 2015).

Lastly, we note that the small jets and spicules discussed in this paper may be relevant to the larger problems of coronal heating and solar wind acceleration. There is evidence that the rapid upward mass transfer in Type II spicules continues as the plasma heats to temperatures in excess of  $10^5$ – $10^6$  K (McIntosh & De Pontieu 2009; Skogsrud et al. 2015). However, there is also skepticism concerning the suggestion that jets and spicules act as a primary source of coronal plasma (Klimchuk 2012, 2015; Judge et al. 2012). Nevertheless, it appears more certain that the *waves* originating in lower atmospheric structures survive as they propagate up into the corona and heliosphere. Similar kinds of nonlinear mode coupling have been proposed to act along open field lines in the solar wind (e.g., Del Zanna et al. 2001; Chandran 2005; Cranmer & van Ballegooijen 2012; Miyamoto et al. 2014), and what we learn about this process in the chromosphere and TR can help improve our understanding of these other regions as well.

The authors gratefully acknowledge Adriaan van Ballegooijen for developing the BRAID code and for decades of valuable collaboration. We also thank Hui Tian, Sean McKillop, Rebecca Arbacher, and the *IRIS* team for their intrepid efforts to identify and characterize the faint, short-lived network jets. This work was supported by NSF SHINE program grant AGS-1540094, NSF Graduate Research Fellowship grant DGE-1144152, and start-up funds from the Department of Astrophysical and Planetary Sciences at the University of Colorado Boulder.

## REFERENCES

- Ahmad, I. A., & Withbroe, G. L. 1977, *Sol. Phys.*, 53, 397  
 Aschwanden, M. J., De Pontieu, B., & Katrukha, E. 2013, *Entropy*, 15, 3007  
 Asgari-Targhi, M., & van Ballegooijen, A. A. 2012, *ApJ*, 746, 81  
 Asgari-Targhi, M., van Ballegooijen, A. A., Cranmer, S. R., et al. 2013, *ApJ*, 773, 111

- Avrett, E. H., & Loeser, R. 2008, *ApJS*, 175, 229
- Banerjee, D., Teriaca, L., Doyle, J. G., et al. 1998, *A&A*, 339, 208
- Beckers, J. M. 1972, *ARA&A*, 10, 73
- Bertschinger, E., & Chevalier, R. A. 1985, *ApJ*, 299, 167
- Bogdan, T. J., Rosenthal, C. S., Carlsson, M., et al. 2002, *Astron. Nachr.*, 323, 196
- Chandran, B. D. G. 2005, *Phys. Rev. Lett.*, 95, 265004
- Cheung, M. C. M., De Pontieu, B., Tarbell, T. D., et al. 2015, *ApJ*, 801, 83
- Cranmer, S. R., & van Ballegoijen, A. A. 2012, *ApJ*, 754, 92
- Cranmer, S. R., van Ballegoijen, A. A., & Edgar, R. J. 2007, *ApJS*, 171, 520
- Culhane, L., Harra, L. K., Baker, D., et al. 2007, *PASJ*, 59, S751
- Del Zanna, L., Matteini, L., Landi, S., et al. 2015, *J. Plasma Phys.*, 81, 3202
- Del Zanna, L., Velli, M., & Londrillo, P. 2001, *A&A*, 367, 705
- De Pontieu, B. 1999, *A&A*, 347, 696
- De Pontieu, B., McIntosh, S. W., Hansteen, V. H., et al. 2007, *PASJ*, 59, S655
- De Pontieu, B., McIntosh, S. W., Hansteen, V. H., et al. 2009, *ApJL*, 701, L1
- De Pontieu, B., Rouppe van der Voort, L., McIntosh, S. W., et al. 2014b, *Science*, 346, 1255732
- De Pontieu, B., Title, A. M., Lemen, J. R., et al. 2014a, *Sol. Phys.*, 289, 2733
- Dewar, R. L. 1970, *Phys. Fluids*, 13, 2710
- Dobrzycka, D., Cranmer, S. R., Raymond, J. C., et al. 2002, *ApJ*, 565, 621
- Feldman, U., Doschek, G. A., & Mariska, J. T. 1979, *ApJ*, 229, 369
- Filippov, B., & Koutchmy, S. 2000, *Sol. Phys.*, 196, 311
- Fletcher, L., Cargill, P. J., Antiochos, S. K., & Gudiksen, B. V. 2015, *Space Sci. Rev.*, 188, 211
- Goldstein, M. L. 1978, *ApJ*, 219, 700
- Hasan, S. S., & van Ballegoijen, A. A. 2008, *ApJ*, 680, 1542
- Heyvaerts, J., & Priest, E. R. 1983, *A&A*, 117, 220
- Hollweg, J. V. 1971, *J. Geophys. Res.*, 76, 5155
- Hollweg, J. V. 1992, *ApJ*, 389, 731
- Hollweg, J. V. 2006, *Phil. Trans. Roy. Soc. A*, 364, 505
- Hollweg, J. V., Jackson, S., & Galloway, D. 1982, *Sol. Phys.*, 75, 35
- Hollweg, J. V., & Kaghashvili, E. K. 2012, *ApJ*, 744, 114
- Jacques, S. A. 1977, *ApJ*, 215, 942
- Jayanti, V., & Hollweg, J. V. 1993, *J. Geophys. Res.*, 98, 19049
- Jess, D. B., Mathioudakis, M., Erdélyi, R., et al. 2009, *Science*, 323, 1582
- Judge, P. G., De Pontieu, B., McIntosh, S. W., et al. 2012, *ApJ*, 746, 158
- Klimchuk, J. A. 2012, *J. Geophys. Res.*, 117, A12102
- Klimchuk, J. A. 2015, *Phil. Trans. Roy. Soc. A*, 373, 20140256
- Kono, S., Yokoyama, T., Toriumi, S., & Katsukawa, Y. 2015, *IRIS-4 Workshop*, poster 19
- Krishna Prasad, S., Banerjee, D., Van Doorselaere, T., & Singh, J. 2012, *A&A*, 546, A50
- Kudoh, T., & Shibata, K. 1999, *ApJ*, 514, 493
- Kukhianidze, V., Zaqarashvili, T. V., & Khutsishvili, E. 2006, *A&A*, 449, L35
- Lamb, H. 1908, *Proc. London Math. Soc.*, 7, 122
- Lamb, H. 1932, *Hydrodynamics* (New York: Dover Publications)
- Lee, M. A., & Roberts, B. 1986, *ApJ*, 301, 430
- Liu, J., McIntosh, S. W., De Moortel, I., et al. 2014, *ApJ*, 797, 7
- Liu, J., McIntosh, S. W., De Moortel, I., et al. 2015, *ApJ*, 806, 273
- Ludwig, H.-G., & Kučinskas, A. 2012, *A&A*, 547, A118
- Lynch, B. J., Edmondson, J. K., & Li, Y. 2014, *Sol. Phys.*, 289, 3043
- Mariska, J. T., & Hollweg, J. V. 1985, *ApJ*, 296, 746
- Mathioudakis, M., Jess, D. B., & Erdélyi, R. 2013, *Space Sci. Rev.*, 175, 1
- Matsumoto, T., & Shibata, K. 2010, *ApJ*, 710, 1857
- Matsumoto, T., & Suzuki, T. K. 2014, *MNRAS*, 440, 971
- Matthaeus, W. H., Wan, M., Servidio, S., et al. 2015, *Phil. Trans. Roy. Soc. A*, 373, 20140154
- McIntosh, S. W. 2012, *Space Sci. Rev.*, 172, 69
- McIntosh, S. W., & De Pontieu, B. 2009, *ApJL*, 706, L80
- Medvedev, M. V., & Diamond, P. H. 1996, *Phys. Plasmas*, 3, 863
- Miyamoto, M., Imamura, T., Tokumaru, M., et al. 2014, *ApJ*, 797, 51
- Mjølhus, E., & Wyller, J. 1986, *Physica Scripta*, 33, 442
- Moore, R. L., Cirtain, J. W., Sterling, A. C., et al. 2010, *ApJ*, 720, 757
- Moore, R. L., Sterling, A. C., Cirtain, J. W., et al. 2011, *ApJL*, 731, L18
- Moriyasu, S., Kudoh, T., Yokoyama, T., et al. 2004, *ApJL*, 601, L107
- Mumford, S. J., Fedun, V., & Erdélyi, R. 2015, *ApJ*, 799, 6
- Murawski, K., Solov'ev, A., Musielak, Z. E., et al. 2015, *A&A*, 577, A126
- Nakariakov, V. M., Roberts, B., & Murawski, K. 1998, *A&A*, 332, 795
- Newkirk, G., Jr., & Harvey, J. 1968, *Sol. Phys.*, 3, 321
- Nuevo, F. A., Huang, Z., Frazin, R., et al. 2013, *ApJ*, 773, 9
- Ofman, L. 2009, *Space Sci. Rev.*, 149, 153
- Ofman, L., Nakariakov, V. M., & DeForest, C. E. 1999, *ApJ*, 514, 441
- Owocki, S. P. 2004, in *EAS Publ. Ser.*, 13, 163
- Pant, V., Dolla, L., Muzumder, R., et al. 2015, *ApJ*, 807, 71
- Paraschiv, A. R., Bemporad, A., & Sterling, A. C. 2015, *A&A*, 579, A96
- Pariat, E., Antiochos, S. K., & DeVore, C. R. 2009, *ApJ*, 691, 61
- Pereira, T. M. D., De Pontieu, B., & Carlsson, M. 2012, *ApJ*, 759, 18
- Perez, J. C., & Chandran, B. D. G. 2013, *ApJ*, 776, 124
- Peter, H. 2013, *Sol. Phys.*, 288, 531
- Raouafi, N.-E., Petrie, G. J. D., Norton, A. A., et al. 2008, *ApJL*, 682, L137
- Roberts, B. 2000, *Sol. Phys.*, 193, 139
- Shibata, K., Nakamura, T., Matsumoto, T., et al. 2007, *Science*, 318, 1591
- Skogsrud, H., Rouppe van der Voort, L., & De Pontieu, B. 2014, *ApJL*, 795, L23
- Skogsrud, H., Rouppe van der Voort, L., De Pontieu, B., & Pereira, T. M. D. 2015, *ApJ*, 806, 170
- Spangler, S. R. 1989, *Phys. Fluids B*, 1, 1738
- Stangalini, M., Giannattasio, F., & Jafarzadeh, S. 2015, *A&A*, 577, A17
- Stein, R. F., & Schwartz, R. A. 1972, *ApJ*, 177, 807
- Sterling, A. C. 2000, *Sol. Phys.*, 196, 79
- Tavabi, E., Koutchmy, S., Ajabshirizadeh, A., et al. 2015, *A&A*, 573, A4
- Threlfall, J., De Moortel, I., McIntosh, S. W., et al. 2013, *A&A*, 556, A124
- Thurgood, J. O., & McLaughlin, J. A. 2013, *Sol. Phys.*, 288, 205
- Tian, H., DeLuca, E., Cranmer, S. R., et al. 2014, *Science*, 346, 1255711
- Tian, H., DeLuca, E., Cranmer, S. R., et al. 2015, *IRIS-4 Workshop*, poster 38
- Tomczyk, S., & McIntosh, S. W. 2009, *ApJ*, 697, 1384
- Tomczyk, S., McIntosh, S. W., Keil, S. L., et al. 2007, *Science*, 317, 1192
- Tsiropoula, G., Tziotziou, K., Kontogiannis, I., et al. 2012, *Space Sci. Rev.*, 169, 181
- Turkmani, R., & Torkelsson, U. 2003, *A&A*, 409, 813
- Uchida, Y., & Kaburaki, O. 1974, *Sol. Phys.*, 35, 451
- van Ballegoijen, A. A., Asgari-Targhi, M., & Berger, M. A. 2014, *ApJ*, 787, 87
- van Ballegoijen, A. A., Asgari-Targhi, M., Cranmer, S. R., et al. 2011, *ApJ*, 736, 3
- Vasquez, B. J., & Hollweg, J. V. 1996, *J. Geophys. Res.*, 101, 13527
- Velli, M., & Liewer, P. 1999, *Space Sci. Rev.*, 87, 339
- Vernazza, J. E., Avrett, E. H., & Loeser, R. 1981, *ApJS*, 45, 635
- Wang, Y.-M., & Sheeley, N. R., Jr. 1995, *ApJ*, 452, 457
- Wang, Y.-M., Sheeley, N. R., Jr., Socker, D. G., et al. 1998, *ApJ*, 508, 899
- Willson, L. A., & Hill, S. J. 1979, *ApJ*, 228, 854
- Woolsey, L. N., & Cranmer, S. R. 2014, *ApJ*, 787, 160
- Woolsey, L. N., & Cranmer, S. R. 2015, *ApJ*, in press, arXiv:1509.00377
- Young, P. R., & Muglach, K. 2014, *PASJ*, 66, S129
- Zhang, J., White, S. M., & Kundu, M. R. 1998, *ApJL*, 504, L127
- Zhdankin, V., Uzdensky, D. A., & Boldyrev, S. 2015, *Phys. Rev. Lett.*, 114, 065002